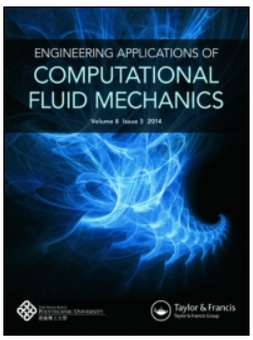

Engineering Applications of Computational Fluid Mechanics

ISSN: 1994-2060 (Print) 1997-003X (Online) Journal homepage: https://www.tandfonline.com/loi/tcfm20

# Mitigation of radial exciting force of rotary lobe pump by gradually varied gap

Yi-Bin Li, Dong-Sheng Guo & Xiao-Bin Li

**To cite this article:** Yi-Bin Li, Dong-Sheng Guo & Xiao-Bin Li (2018) Mitigation of radial exciting force of rotary lobe pump by gradually varied gap, Engineering Applications of Computational Fluid Mechanics, 12:1, 711-723, DOI: 10.1080/19942060.2018.1517053

**To link to this article:** https://doi.org/10.1080/19942060.2018.1517053



Published online: 07 Sep 2018.

ENGINEERING APPLICATIONS OF COMPUTATIONAL FLUID MECHANICS
2018, VOL. 12, NO. 1, 711–723
https://doi.org/10.1080/19942060.2018.1517053

Taylor & Francis
Taylor & Francis Group



# Mitigation of radial exciting force of rotary lobe pump by gradually varied gap

Yi-Bin Li[a,b], Dong-Sheng Guo [a] and Xiao-Bin Li[c]

[a]College of Energy and Power Engineering, Lanzhou University of Technology, Lanzhou, People's Republic of China ; [b]Key Laboratory of Fluid Machinery and Systems, Gansu Province, People's Republic of China ; [c]Sino-French Institute of Nuclear Engineering and Technology, Sun Yat-Sen University, Zhuhai, People's Republic of China

**ABSTRACT**

This paper presents a new structure of a rotary lobe pump cavity with gradually varied gap to mitigate the magnitude and fluctuation of the radial exciting force on the rotor. The geometry of the rotary lobe pump cavity is specially designed, so that the gap between the rotor and cavity is gradually changed during the rotors' engaging. The flow in this geometry is numerically studied, and its effect on the pressure pulsation and radial exciting force is analysed, based on the dynamic mesh and local mesh reconstruction. Also, the mechanism of the mitigation of radial exciting force is briefly discussed. The value of the gap is an addition of gradually varied gap $r$ ($0 \sim r_{max}$) and the base gap (original constant gap: 0.2 mm). As for the results, it is found that as the varied gap $r_{max}$ value increases, the intensity of the reverse rotating vortex at the outlet decreases, and the secondary flow pulsation of the outlet section is effectively weakened. When $r_{max} = 0.1$ mm, the radial exciting force in the $y$-direction on the rotor is reduced by 12% comparing with the equal gap, and the radial exciting force pulsation coefficient is 0.31. Meanwhile, the radial exciting force in the $x$-direction is reduced by 19% accordingly. The gradually varied gap cavity can effectively reduce the peak value of the pressure pulsation at outlet, weakening the influence of the rapid change of the outlet pressure on the radial exciting force. It is found that an optimal $r_{max}$ of $0.1 \sim 0.15$ mm has a remarkable effect on the mitigation of pressure pulsation and radial exciting force.

**ARTICLE HISTORY**
Received 8 April 2018
Accepted 24 August 2018

**KEYWORDS**
Rotary lobe pump; pump cavity; gradually varied gap; radial exciting force; flow pulsation; numerically studied

## 1. Introduction

Rotary lobe pump is a positive displacement pump, one of rotary volumetric pumps, widely used in chemical, food, and pharmaceutical industries (Dickenson, 1995). The rotary lobe pump takes the advantage of its simplicity of high flow rate, components and low maintenance costs, *etc*. In the working process of the rotary lobe pump, the volume of the suction and drainage cavity will change periodically with the rotation of the transmission shaft. The operating mechanism of the rotary lobe pump determines that it generates flow and pressure pulsation in the operation. As the fluid pressure at the pump outlet fluctuates, the radial exciting force also shows a periodic change, exerting an alternating load on the drive shaft. As a result, the service lifespan of the drive shaft is reduced, so that all components of the entire system will cause serious damage. Therefore, how to reduce the flow fluctuation and pressure pulsation at outlet of the rotary lobe pump, so as to improve the stability of the whole system, becomes an important issue.

From the perspective of fluid mechanics, identifying the elaborate internal flow characteristics and visualizing flow state are prerequisite for evaluating the performance of the pump comprehensively. However, as we have known that the rotary lobe pump is a kind of positive displacement pump, conveying fluid using the principle of rotation. Since the cavity geometry where the fluid occupies changes during the rotation, it is very hard to comprehend the physical phenomenon appearing in such complicated operating processes.

Recently, as the computational fluid dynamics (CFD) technique develops, many researchers have introduced the dynamic mesh to deal with the computational domain changes, thus the numerical calculation of the flow field inside the rotary lobe pumps was realized (Mimmi & Pennacchi, 1999; Valdès, Barthod, & Perron, 1999; Vogelsang, Verhülsdonk, Türk, & Hörnig, 1999). For reducing the flow rate fluctuation, Costopoulos, Kanarachos, and Pantazis (1988) designed the spur gear pumps with tooth profiles. With the required flow rate function, an integral synthesis procedure was presented by Tong and Yang (2005). A dimensionless flow rate expression called 'specific flow rate' is used in the lobe pump. Wang, Jiang, and Cai (2015) proposed a novel

**CONTACT** Dong-Sheng Guo guodongsheng1316@163.com

circular arc claw rotor profile, the gas flow in the claw vacuum pump was simulated numerically and the pressure distribution which is caused by claw rotors' gas pressure was calculated carefully. The flow of the involute leaf lobe pump is a periodic parabolic function (Mimmi & Pennacchi, 1994). Sun, Jia, Xing, and Peng (2018) analysed the effect of reflux on the performance of the roots blowers. They found that the result of CFD simulation is in good agreement with that of the experiment. Peng, Gui, and Fan (2018) calculated the flow of the complex oil of a hypoid gear when it is splashed in the tank. They found that the numerical method can accurately predict the flow of the complex oil in the hypoid gearbox, at the same time it can also provide a numerical method for studying the oil flow and churning loss in the axle shell of the real vehicle. Huang and Liu (2009) simulated the flow in a roots blower with three lobes using the $k$–$\epsilon$ turbulence model and compared with semi-empirical formulas calculation results due to their uneven outlet flow. It was claimed that during the meshing process of two rotors, the amplitude of the periodical function varies due to the contact point position change (Yang & Tong, 2002). Ma, Luo, Zhang, Zhou, and Deng (2017) researched the combined valves' dynamic characteristics in reciprocating oil–gas multiphase pump by the CFD method with the dynamic mesh. They found that the valve plates may grab or rebound and then vibrate after reaching the elevator limiter, and the lag angle of one cycle remains 3° under different working conditions.

A new type of variable trochoid ratio rotor profile was proposed by Hwang and Hsieh (2006), and the method of achieving sealing performance and higher volumetric efficiency was investigated. Hsieh and Hwang (2015) further proposed a new curve of cavity. The curve was formed around the long axis of ellipse roller arc rolling endpoint using an elliptic roller track. Then the rotary lobe pump based on the curve model was simulated, and the results showed that the flow characteristics were improved. Kang and Vu (2014) developed a new kind of rotor profile that obviously improved the performance of the pump. Their study evaluated the four profiles' performance by the volume calculation and the flow field analysis with consideration of the number of pump lobes. The results demonstrated that the shapes of rotors affected the pump performance observably. Li, Jia, Meng, Shen, and Sang (2013) numerically investigated the internal flow field in a tow-vane involute rotary lobe pump using the RNG $k$-$\epsilon$ turbulence model and dynamic grids. The influence of the pressure angle on the transient characteristics of the flow field inside the rotary lobe pump is analysed. Turbulence modeling's influence on the CFD prediction of local velocity fields of twin-screw compressors was studied by Kethidi, Kovacevic, Stosic, and Smith (2011). Arjeneh, Kovacevic, Rane, Manolis, and Stosic (2015) surveyed the local pressure loss in the suction chamber of the screw compressor and predicted the pressure loss in the CFD calculation using the surveyed results. Kovacevic, Stosic, Mujic, and Smith (2007) described the combination mechanism of CFD and other design software in which interactive control of the entire design process of screw compressor was obtained through an integral management system, and the described methods can be applied to all types of twin-rotor rotary machines not only the compressor. Campo, Castilla, Raush, Montero, and Codina (2012) proposed a simplified two-dimensional numerical calculation to study the cavitation effect in the external gear pump. The above studies indicated that the flow features and the flow-induced mechanical response were critical to the flow conditions and the geometries. Alemi, Nourbakhsh, Raisee, and Najafi (2015) used the $k$–$\omega$ turbulence model to simulate the casings concentric at 180°, 270°, and 360° from the tongue, showing that the lowest radial force appears in the 270° concentric volute within the entire flow rate range. Zhang, Ma, Hong, Yang, and Fang (2017) numerically investigated the flow ripple characteristics in the piston pump. At the same time, the pump flow conditions were tested using a pump flow ripple test bed. The results show that the simulation results are in good agreement with the experimental.

In the present paper, a new type of pump cavity with gradually varied gap is proposed. The gap between the high-pressure cavity and the rotor is designed as a gradually varied gap, and the value of the gradient section and the gap value satisfy a specific mathematical relationship. This configuration is to improve the flow performance and mitigate the influence of pressure fluctuation, hereby reduce the radial exciting force on the rotor.

This paper has simulated the unsteady performance in a three-cycloid rotary lobe pump based on the dynamic mesh techniques in the commercial CFD software ANSYS Fluent, especially focusing on the distribution of the radial exciting force in gradually varied and equal gap of the pump cavity.

## 2. Rotor geometry mathematical model

### 2.1. Mathematical model and profile equation

The present paper introduces a pump rotor adopting a combined profile of three-leaf inner cycloid and outer cycloid. As shown in Figure 1, assume that the angle between $OO_{b1}(O_{b2})$ and the $x$-axis is $\theta$ (Figure 1(a)). AB segment is outer cycloid (colored red), BC segment is inner cycloid (colored green), and these two segments constitute 1/6 part (60°) of the rotor's profile

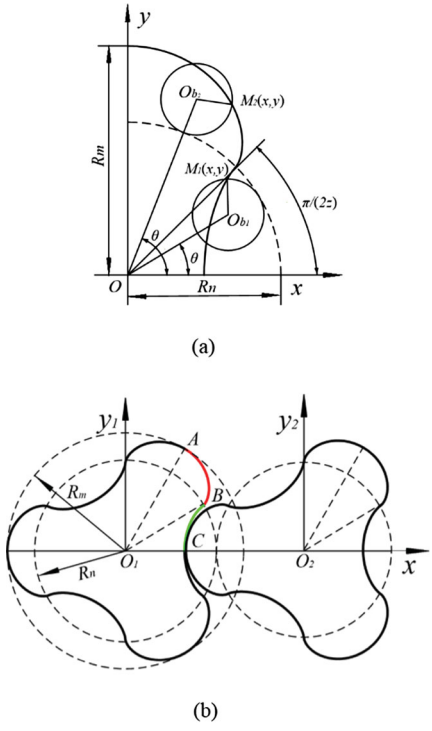


**Figure 1.** Rotor profile of rotary lobe pump. (a) Cycloid formation principle. (b) Geometric relation of the conjugate rotor.

(Figure 1(b)). The equations of outer and inner cycloid profile are expressed as

$$x = \frac{(2z+1)R_m}{2(z+1)}\cos\theta + \frac{R_m}{2(z+1)}\cos[(1+2z)\theta]$$
$$y = \frac{(2z+1)R_m}{2(z+1)}\sin\theta + \frac{R_m}{2(z+1)}\sin[(1+2z)\theta] \quad (1)$$

Definition: $\pi/(2z) \le \theta \le \pi/z$.

$$x = \frac{(2z-1)R_m}{2(z+1)}\cos\theta - \frac{R_m}{2(z+1)}\cos[(1-2z)\theta]$$
$$y = \frac{(2z-1)R_m}{2(z+1)}\sin\theta - \frac{R_m}{2(z+1)}\sin[(1-2z)\theta] \quad (2)$$

Definition: $0 \le \theta \le \pi/(2z)$. Here, $R_m$ is the rotor tip radius, $R_n$ is the pitch radius, $z$ is the number of rotors.

Figure 2 shows the structural design of the gradually varied gap, and the high-pressure side of the pump cavity is designed as a function of the gradually varied gap (colored red) as the gradient segment (while the original profile with constant gap is colored blue), and the values of $R_1$, $R_2$ and $R_3$ are set to increase the inner diameter of the pump cavity linearly, and the opening angle of the transition section is 60°, the equation is expressed as:

$$x = R \cdot \cos(30 + t \cdot \delta)$$
$$y = R \cdot \sin(30 + t \cdot \delta) \quad (3)$$

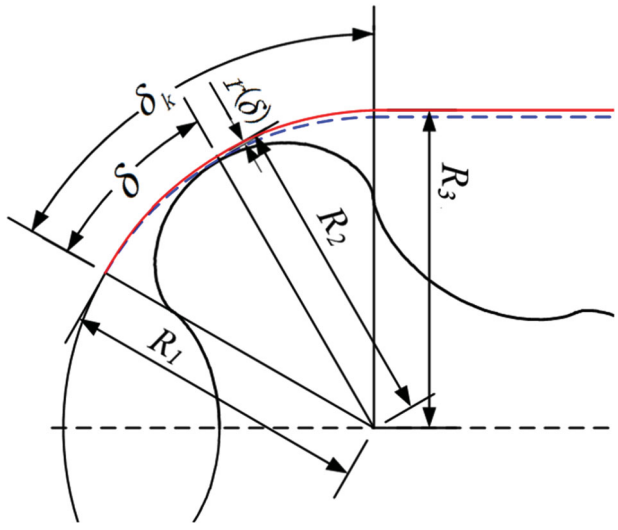


**Figure 2.** Structure design with the gradually varied gap.

where $0 \le \delta \le \pi/3$, $R = R_m + r_{max} \cdot t$, $0 \le t \le 1$, $R_m$ is the rotor tip radius. $r$ is the value of gradual change of the pump cavity. In this paper, the values of $r_{max}$ are 0, 0.05, 0.1, 0.15, 0.2 and 0.25 mm, respectively, and the original constant gap is 0.2 mm. So the final gap is the sum of the original constant gap and the varied $r$.

### 2.2. Rated parameters of the model

In this paper, the influence of the radial gap on its performance is studied, so the axial gap is ignored in the calculation. Considering the symmetry of the three-leaf rotary lobe pump, the radial cross-section flow in the three-dimensional model is the same as that in the two-dimensional. In order to speed up the convergence of numerical simulation, the computational model of the rotary lobe pump is simplified into a two-dimensional planar model. The main structure and operating condition parameters of the pump are shown in Table 1.

## 3. Numerical calculation method

### 3.1. Meshing and dynamic mesh model

As shown in Figure 3, the whole grids area is divided into inlet part, outlet part and rotor part. Because the meshing gap between the rotors and the gap between rotor and pump cavity are very small, all of the parts adopt a quadrilateral mesh structure. Grid and time-step-independent verification can be guaranteed, as shown in Figure 4(a), the result error between $2.1\times10^5$ grid number mesh and $2.2\times10^5$ is less than 0.23%, meanwhile, the error between $2.2\times10^5$ grid number mesh and $2.3\times10^5$ is less than 0.043%. But the error between $1.8\times10^5$ grid

**Table 1.** Structure parameters and work condition of pump.

| Blade numbers | Tip radius ($R_m$/mm) | Center distance ($L$/mm) | Axial length of rotor ($l$/mm) | Inlet and outlet diameter ($d$/mm) | Rated speed $n$/(r/min$^{-1}$) |
|---|---|---|---|---|---|
| 3 | 79.8 | 120 | 100 | 80 | 420 |

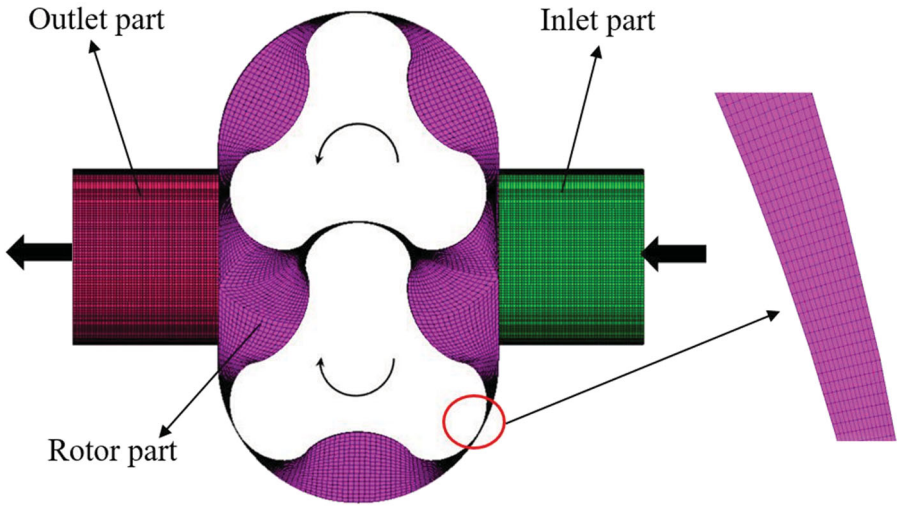


**Figure 3.** Mesh model of the pump.

number mesh and $2.2\times10^5$ is more than 1.6%, so that the grid-independent results adopted $2.2\times10^5$ cells.

The independent verification of time step was used to compare the simulation results under different three time steps. Figure 4(b) shows the calculated results of the $2.2\times10^5$ grids with the different three time steps. The error of the different three time steps was less than 0.15%, so the time step would be adopted is $1\times10^{-5}$ s. The negative volume will occur and the simulation results would go wrong when the time step was set bigger than $1\times10^{-5}$ s. The two rotors are set as the moving boundary, the two ends of the pump body are set as rigid bodies, and the motion mode of the rotor is given by user-defined functions.

In the ANSYS Fluent, the dynamic mesh model is used to calculate the flow of basin shape change with time due to the movement of the basin boundary. For the rotary motion of the rotary lobe pump rotor, the calculation of the next time step is determined by the calculation result of the current time step. The deformation of the volume grids of each time step is based on the new position of the boundary condition. The dynamic mesh computing model (FLUENT 15.0 Documentation 2013) is expressed as

$$\frac{\mathrm{d}}{\mathrm{d}t}\int_V \rho\varphi \mathrm{d}V + \int_{\partial V} \rho\varphi(\boldsymbol{u}-\boldsymbol{u}_s)\mathrm{d}A = \int_{\partial V}\Gamma\nabla\varphi \mathrm{d}A + \int_V S_\varphi \mathrm{d}V \tag{4}$$

where the $\rho$ is the density of the fluid, $\boldsymbol{u}$ is the velocity vector of the fluid, $\boldsymbol{u_s}$ is the deformation velocity for dynamic mesh, $\Gamma$ is the diffusion coefficient, $S_\varphi$ is the flux source term and $\partial V$ is the boundary of the control volume.

The first term is the first-order backward difference and the equation is expressed as

$$\frac{\mathrm{d}}{\mathrm{d}t}\int_V \rho\varphi \mathrm{d}V = \frac{(\rho\varphi V)^{n+1}-(\rho\varphi V)^n}{\Delta t} \tag{5}$$

where $n$ and $n+1$ are the current and immediate time steps, respectively, which are used to achieve the progress of the time step.

The volume $V^{n+1}$ of the $n+1$ step is

$$V^{n+1} = V^n + \frac{\mathrm{d}V}{\mathrm{d}t}\Delta t \tag{6}$$

where the time step is determined by $\Delta t = \mathrm{CFL}\Delta x/\lambda_{max}$, and CFL is the Courant number, $\Delta x$ represents the distance of the grids and $\lambda_{max}$is the maximum velocity scale. So, the time step adopted is $1\times10^{-5}$ s.

Figure 5 shows the mesh reconstruction of the deformed region. Layer $j$ is a grid layer adjacent to the moving boundary. A new unit layer is determined by the height $h$ of the layer $j$ or is formed by merging layer $j$ with the adjacent layer $i$. Assuming that the layer $j$ is being inflated, and the expansion height $h$ allowed by FLUENT would be:

$$h_{\min} = (1+\alpha_s)h_{ideal} \tag{7}$$

where the cell layer $j$ is the minimum cell height $h_{min}$, $h_{ideal}$ is the ideal cell height, $\alpha_s$ is the layer split factor.

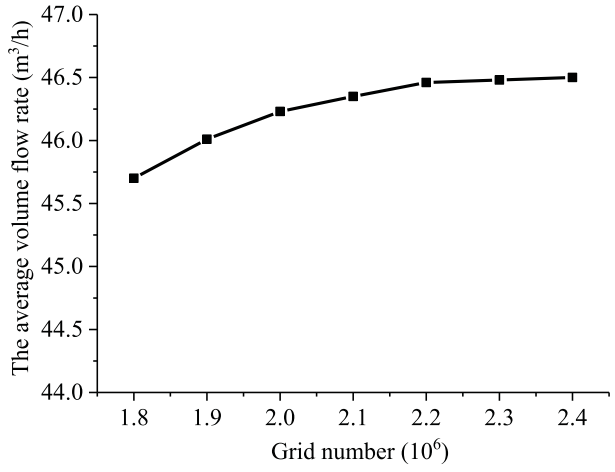


(a)

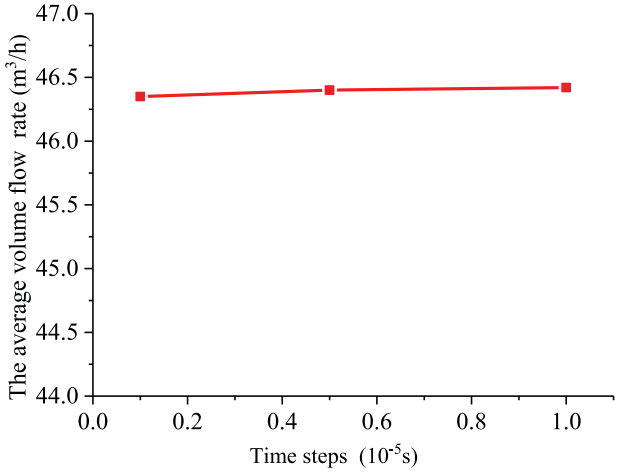


(b)

**Figure 4.** Grid and time-step-independent verification. (a) The independence of the grids. (b) The independence of the time steps.

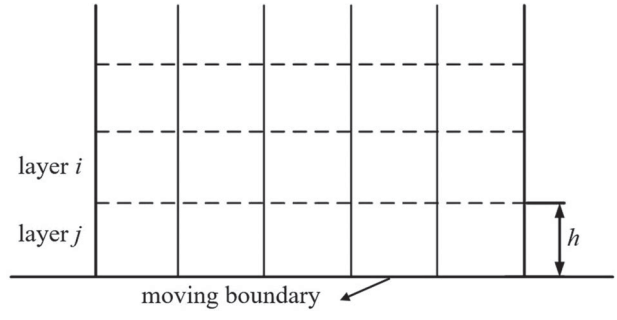


**Figure 5.** Mesh reconstruction of the deformed region.

Note that when $h_{\min} > (1+\alpha_s)h_{ideal}$, the unit will split according to a predefined height, at which point the unit height in the layer $i$ is the ideal height $h_{ideal}$. Conversely, if the unit volume of the layer $j$ is being compressed, the compressed unit surface will form a new unit layer on the unit surface of the adjacent layer.

### 3.2. Governing equation and turbulence model

The turbulence parameters were obtained by Reynolds Average Navier–Stokes equation group, where the RNG $k$–$\epsilon$ turbulence model and implicit solver was used. The coupling of pressure and velocity adopted the PISO algorithm. The tensor form of the control equations is as follows:

$$\frac{\partial \rho}{\partial t} + \frac{\partial(\rho u_i)}{\partial x_i} = 0 \tag{8}$$

$$\frac{\partial \rho}{\partial t}(\rho u_i) + \frac{\partial}{\partial x_j}(\rho u_i u_j) = -\frac{\partial p}{\partial x_i} + \frac{\partial}{\partial x_j}\left(\mu\frac{\partial u_i}{\partial x_j} - \rho\overline{u'_i u'_j}\right) + S_i \tag{9}$$

where $u_i$, $u_j$ are the average velocity component, $p$ is the average pressure of fluid, $\mu$ is the dynamic viscosity coefficient, and $\rho$ is the density of the fluid.

The RNG $k$–$\epsilon$ turbulence model was proposed by Yakhot and Orszag (1986), and the equations are as follows:

$$\frac{\partial(\rho k)}{\partial t} + \frac{\partial(\rho k u_j)}{\partial x_j} = \frac{\partial}{\partial x_j}\left[\alpha_k \mu_{eff}\frac{\partial k}{\partial x_j}\right] + G_k + \rho\varepsilon \tag{10}$$

$$\frac{\partial(\rho\varepsilon)}{\partial t} + \frac{\partial(\rho\varepsilon u_i)}{\partial x_i} = \frac{\partial}{\partial x_j}\left[\alpha_\varepsilon \mu_{eff}\frac{\partial \varepsilon}{\partial x_j}\right] + G_{1\varepsilon}\frac{\varepsilon}{k}G_k - G_{2\varepsilon}\rho\frac{\varepsilon^2}{k} \tag{11}$$

$$\mu_{eff} = \mu + \mu_t \tag{12}$$

$$\mu_t = \rho C_\mu \frac{k^2}{\varepsilon} \tag{13}$$

where $k$ is the turbulent kinetic energy, $\mu_{eff}$ is the effective viscosity coefficient, $C_\mu$, $\alpha_k$ and $\alpha_\epsilon$ are empirical constant, $C_\mu = 0.0845$, $\alpha_k = 1.39$ and $\alpha_\epsilon = 1.39$, $C_k$ is the turbulent kinetic energy generating term, $\epsilon$ is the turbulent dissipation. In the Fluent, $C_{\epsilon 1} = 1.42$, $C_{\epsilon 2} = 1.68$ are the default constant.

## 4. Test verification of the numerical calculation

The test data for the rotary lobe pump are shown in Table 2. The performance test of the rotary lobe pump through a closed test loop is shown in Figure 6. Testing instrument included pressure transmitter, JN338

torque instrument, RDC2512B type low resistance measuring instrument, temperature measuring instrument (including sensor), BK-1 axial force sensor, JW-3 torque meter, Electromagnetic Flowmeter, electric balance valve, etc. The performance test was carried out according to the GB/T12785 criterion under the condition of normal temperature and clear water. The inlet pressure was controlled by adjusting the manual ball valve so as to change the inlet and outlet pressure difference.

During the test, the pressure difference between the inlet and outlet was controlled by adjusting the manual ball valves in turn. At the same time, the outlet flow pulsation, pressure pulsation and rotor radial exciting force were monitored. While in the simulation, the inlet and outlet of the pump adopt pressure boundary conditions, and the inlet and outlet pressure values were given respectively.

The test data for the rotary lobe pump are shown in Table 2.

**Table 2.** Test at different operating conditions.

| Inlet (kPa) | Outlet (MPa) | Differential (MPa) |
|---|---|---|
| 1.6 | 0.106 | 0.104 |
| 2.7 | 0.199 | 0.196 |
| 3.5 | 0.308 | 0.305 |
| 4.0 | 0.416 | 0.412 |
| 4.6 | 0.501 | 0.495 |
| 4.6 | 0.598 | 0.593 |
| 5.6 | 0.701 | 0.695 |
| 5.5 | 0.797 | 0.792 |

The efficiency of the rotary lobe pump consists of three parts: mechanical efficiency $\eta_m$, volumetric efficiency $\eta_v$ and hydraulic efficiency $\eta_h$. The equation is

$$\eta = \eta_m \eta_v \eta_h = \frac{\Delta p Q}{M\omega} \tag{14}$$

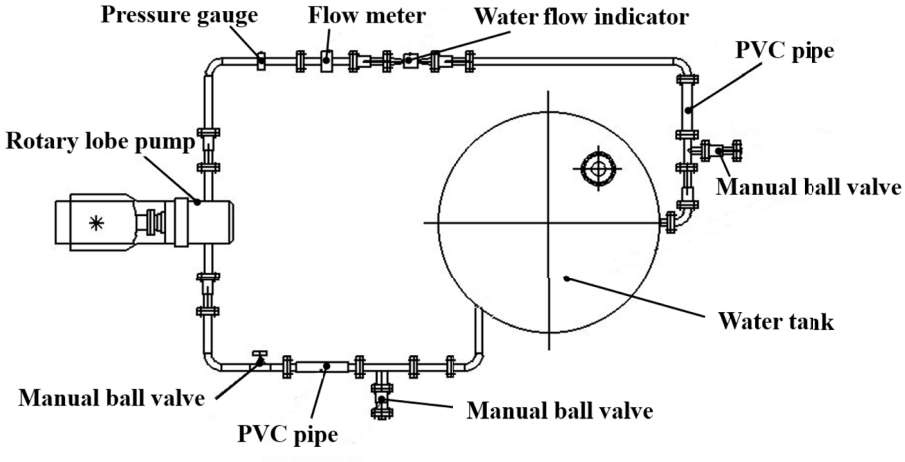


(a)

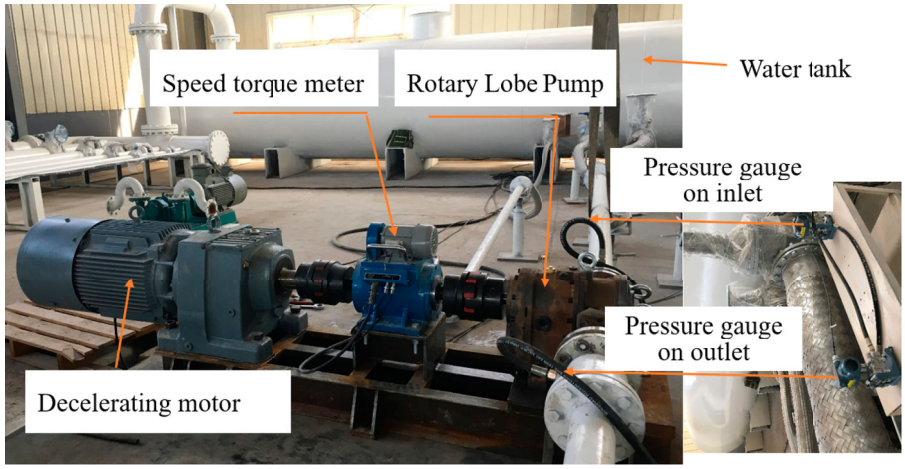


(b)

**Figure 6.** Closed testing loop.

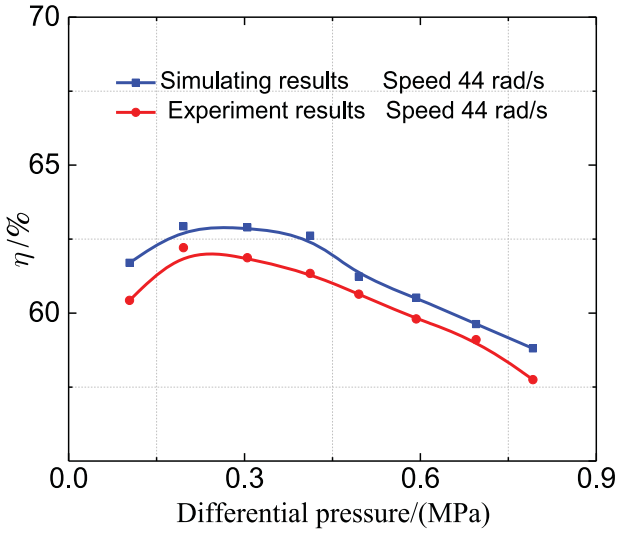


(a)

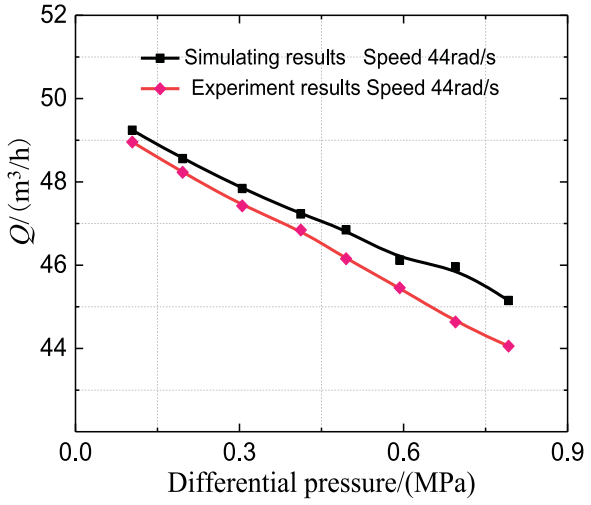


(b)

**Figure 7.** Comparison between the performance test and numerical prediction. (a) Efficiency–pressure difference curve. (b) Flow–pressure difference curve.

where $M$ is the torque of rotors (N·m), $\omega$ is the angular speed (rad/s). $Q$ is the volume flow rate ($m^3/s$).

Figure 7 shows the efficiency/pressure relationship and the volume flow rate/pressure relationship curves obtained from both numerical prediction and experiment of the rotary lobe pump. The results show that under the different pressure drops at the inlet and outlet of the pump, the numerically calculated efficiency values are higher than the experimental values, the errors are all within 3%, and the volume flow rate obtained by numerical calculation is in good agreement with the experimental values. With the increase of the pressure difference between the inlet and outlet, the deviation of

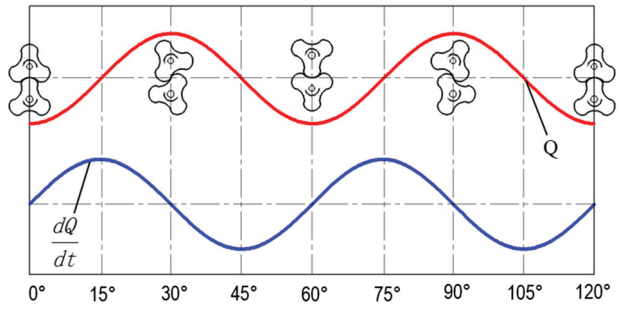


**Figure 8.** Theoretical flow pulsation characteristics of the outlet.

the volumetric flow rate values between experimental and numerical prediction gradually increases. The main reason is that the pressure difference has a great influence on its volumetric efficiency, and with the pressure difference increases, the volume loss increases sharply. In addition, numerical predictions and experimental errors due to numerical calculations ignore the mechanical losses caused by bearings, gears, mechanical seals, etc., as well as other error values that simplify the two-dimensional model of the rotary lobe pump. The RNG $k$–$\epsilon$ turbulence model was used to predict the performance of the rotary lobe pump having good accuracy and the reference value.

## 5. Results and analysis

### 5.1. Effect of the gradually varied gap structure on the flow characteristics

The conjugate rotor generates periodic flow pulsation, which results in vibration and noise of the unit. Therefore, the instantaneous flow pulsation of the pump directly affects the stability of the system operation. As shown in Figure 8, the red curve is the pulsating curve of the theoretical flow rate at the outlet of the rotary lobe pump. In the 1/3 cycle, the outlet flow produces two peaks at 30° and 90°, respectively, and the flow acceleration d$Q$/d$t$ curve also produces two peaks respectively (colored blue).

Figure 9 shows the effect of different gradually varied gap on the flow pulsation at the outlet of the pump in one cycle. The results show that there is a difference between the theoretical flow and the numerical prediction of the pulsating curve of the outlet flow. When $r_{max} = 0$ (means the condition with only the original constant gap), there is a secondary flow pulsation at the peak of the pulsation pump outlet flow, when $r_{max} = 0.05$ mm, the secondary flow pulsation at the outlet of the pump is significantly attenuated, and when $r_{max} = 0.1$ mm, the gradually varied gap effectively inhibits the secondary flow pulsation at the peak value of flow pulsation of

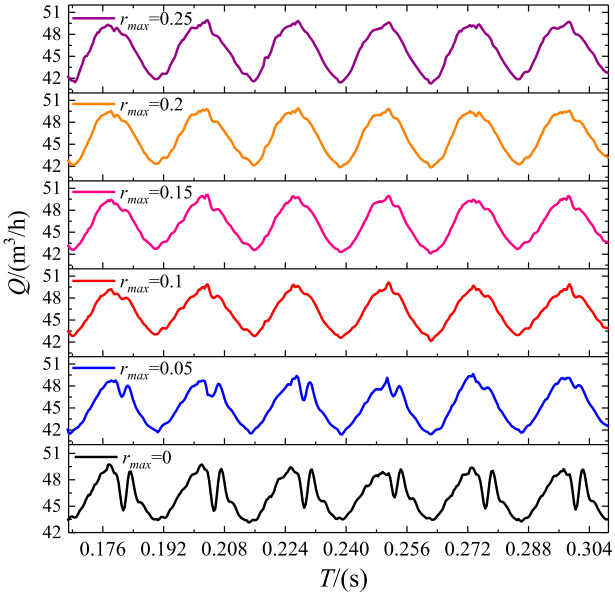


**Figure 9.** Effect of the gradually varied gap on flow pulsation of outlet in one cycle of numerical results.

outlet. With the increase of $r_{max}$ value, the outlet flow pulsation produces a sharp point at the extremum, and the amplitude of the outlet flow pulsation increases gradually. When $r_{max} = 0.1 \sim 0.15$ mm, the flow pulsation at the outlet of the pump is relatively smooth, and the flow pulsation curve obtained by numerical prediction is in good agreement with the theoretical flow pulsation curve.

Figure 10 shows the velocity vector field of the outlet of the pump. There are two counter-rotating vortexes on the outlet region of A and B, respectively. As shown in Figure 10(b), due to the synchronous meshing effect of the two rotors, the fluid has a constrained flow area in the middle of the outlet (shown in the red dotted area). It is easy to form a jet flow region and a velocity gradient occurs, so that a local low-pressure region is easily formed at the region of A and B, resulting in two reversely rotating vortexes. The vortex blocks the fluid at the outlet of the pump, causing local loss of the outlet section to increase. The vortex A and B at the outlet of the pump is the main cause of the secondary flow pulsation at the peak pulsation of the pump outlet flow. With the increasing $r_{max}$ value of the gradually varied gap and when the gap $r_{max} \geq 0.1$ mm, the intensity of the counter-rotating vortex generated at the outlet sections A and B reduces and the secondary flow pulsation of the outlet section is effectively controlled.

### 5.2. Effect of the gradually varied gap on the static pressure distribution in the pump

Figure 11 shows the internal static pressure distribution in the pump of gradually varied and equal gap with different rotation angles. A, B, C and D are transition cavities at different angles. When the gradually varied gap is about to open, the static pressure in transition cavity of the pump is not different from the inlet pressure. With the opening of the gradually varied gap, when the impeller turns around 0°, some fluids of the high-pressure cavity have been flowing into the transition cavity through the gradually varied gap. However, the pressure rise in

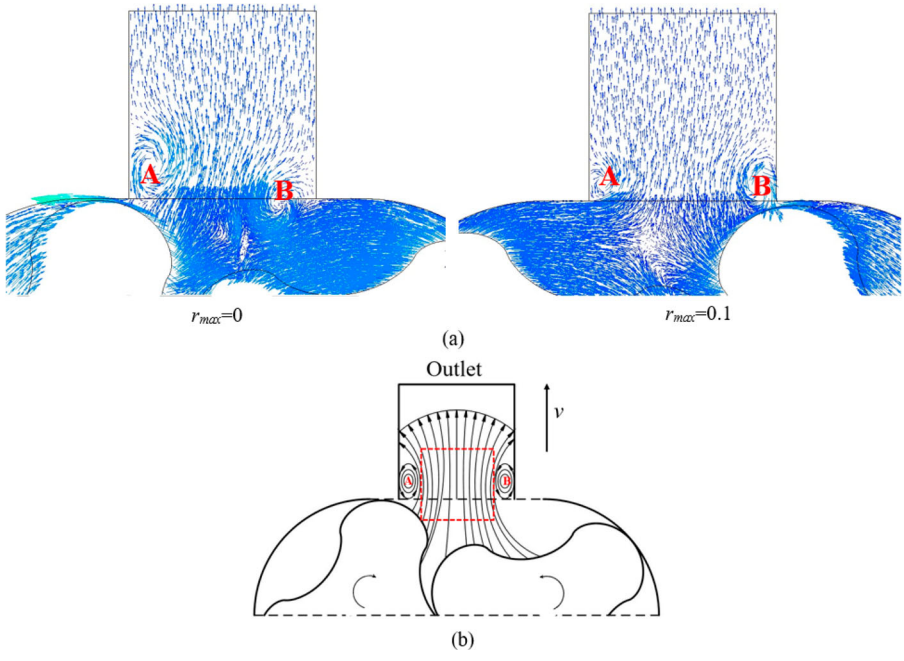


**Figure 10.** Effect of the gradually varied gap on the local vortex of the outlet. (a) $r_{max} = 0.1$. (b) $r_{max} = 0$.

the transition cavity is limited due to the influence of liquid reflux on the high-pressure side. When the impeller turns around 30°, it can be seen that the pressure in the transition cavity increases obviously and closes to the pressure at the high-pressure side. At the same time, the fluid of high-pressure side continues to average pressure by reflux. When the impeller turns around 45°, it can be seen that the pressure in the transition cavity has reached or even exceeded the pressure of the high-pressure side due to the closed backlog of the volume and the rotor rotation work. Therefore, it can be seen that with gradual opening of the gradually varied gap and constant back pressure equalization of the high-pressure side fluid, the pressure in the left transition cavity and the high-pressure side are basically similar and reach steady-state equilibrium within one cycle. As the rotor rotates continuously, the same changes repeated, and the variation of the internal pressure in the volume of the right unit is the same as that in the left unit.

Figure 11(b) shows the pressure distribution of the internal flow field of the rotary lobe pump with equal gap structure at different rotation angles. Comparing with Figure 11(a), it can be found that the pressure distribution of the flow field in the transition cavity does not change obviously with the rotation of the rotor in the equal gap structure. When the impeller rotates through 45°, the pressure in the transition cavity has already exceeded the pressure on the high-pressure side due to the momentary opening of the gap. Due to the effect of instantaneous pressure relief, the rotor will receive a large reflux shock effect, the amplitude of the radial exciting force of the high-pressure end to the rotor and the internal flow noise of the lobe pump increase greatly.

### 5.3. Effect of the gradually varied gap on the radial exciting force $F_r$

With the periodic rotation of the rotor, the flow pulsation at the outlet of the pump induces periodic pressure pulsation, which acts directly on the conjugate rotor and presents periodic alternating load, that is, the radial exciting force on the rotor. Now define the radial force pulsation coefficient as

$$K = \frac{F_{\max} - F_{\min}}{F_{ave}} \tag{15}$$

where $F_r$ is the radial exciting force, $F_{max}$ is the maximum radial exciting force, $F_{min}$ is the minimum radial exciting force, $F_{ave}$ is the average radial exciting force. The components of the radial exciting force pulsation coefficient $K$ in the $Oxy$ plane are denoted by $K_x$ and $K_y$, respectively.

#### 5.3.1. Effect of the gradually varied gap on the radial exciting force in the y-direction

Figure 12(a) shows the effect of the gradually varied gap on the pulsation amplitude of the radial exciting force in the $y$-direction. When $r_{max} = 0$ mm, the pulsation amplitude of the $y$-direction of the rotor in the high-pressure side of the rotor is larger, and the maximum radial exciting force reaches 7.6 kN, and the direction is the negative of the $y$-axis. At this time, the radial force pulsation coefficient reaches the peak point $K_{ymax} = 0.66$ (as shown in Figure 13), which corresponds to the peak of the flow acceleration (the blue curve in Figure 8). At this point, $dQ/dt$ reaches the peak point. When $r_{max} = 0.1$ mm, the amplitude of the radial exciting force pulsation of the high-pressure end of the gradient cavity is significantly lower, and the maximum radial exciting force is 6.7 kN,

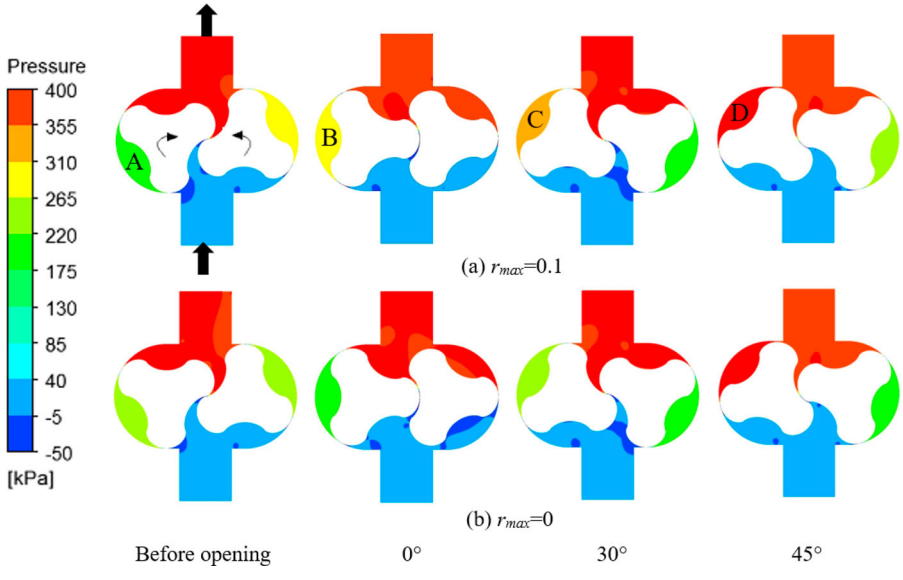


**Figure 11.** Static pressure distribution in the pump.

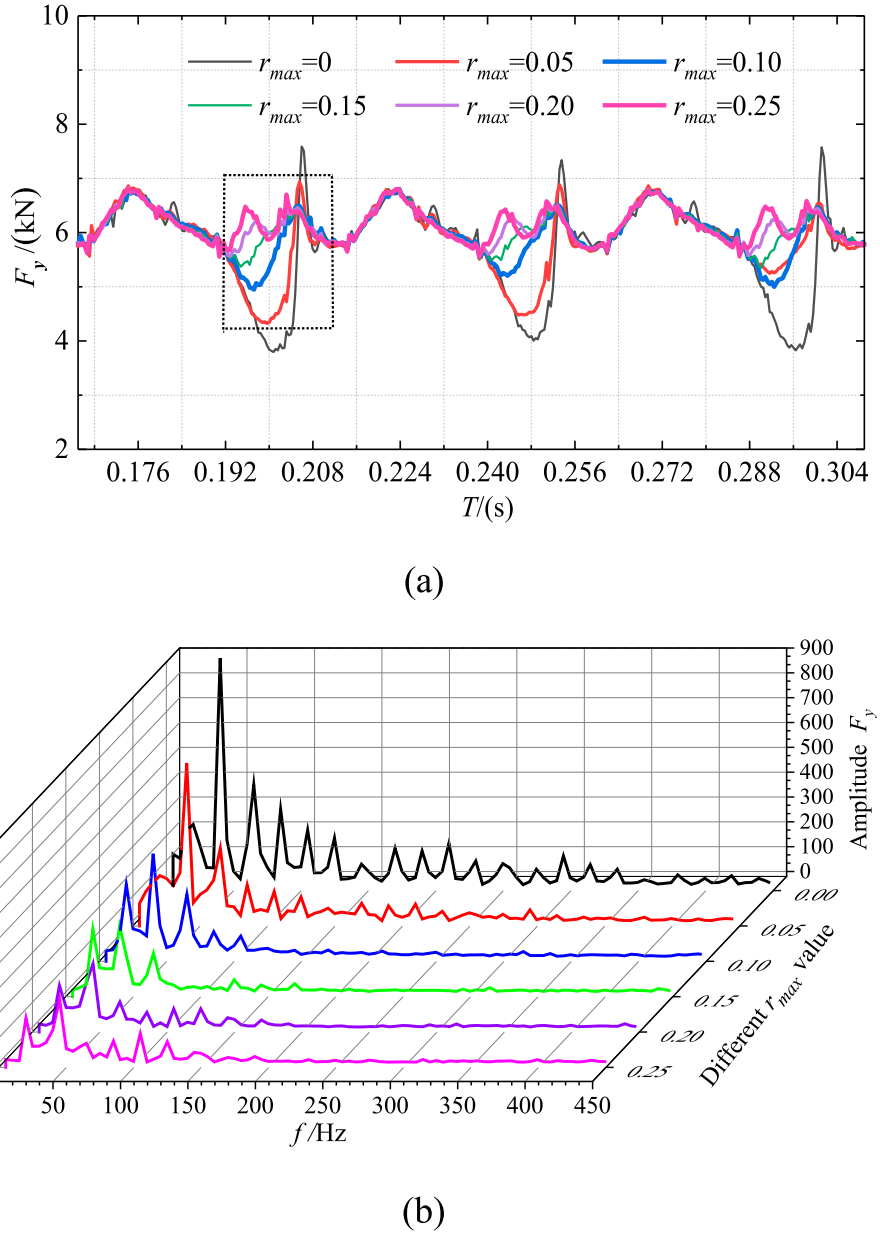


**Figure 12.** Pulsation characteristics of the radial force in the *y*-direction of the rotor.

which is 12% less than the radial exciting force value of the equal gap. The radial exciting force pulsation coefficient is 0.31.

With the increase of the $r_{max}$ value, the pulsation amplitude of the *y*-direction radial exciting force loaded on the rotor at the high-pressure end gradually decreases, reaches the minimum value at $r_{max}$ is 0.15 mm, and then gradually increases. When $r_{max}$ is changed in the range of 0.1 ~ 0.15 mm, the influence of the $r_{max}$ value on the pulsation coefficient of the radial force in the *y*-direction is not remarkable.

Figure 12(b) shows the frequency domain diagram of $F_y$ pulsation of different gradually varied gap. It can be seen that the main frequency of the radial exciting force pulsation at the monitoring point is near 42 Hz, which is twice of the theoretical calculation. This is because the phases are staggered when the two rotors rotate, while the maximum value of the main frequency amplitude of the monitoring point appears at $r_{max} = 0$, and then decreases with the increase in the value of $r_{max}$. The results show that the gradually varied gap can effectively inhibit the pulsation intensity of $F_y$.

### 5.3.2. Effect of the gradually varied gap on the radial exciting force in the x-direction

Figure 14(a) shows the effect of the gradually varied gap on the pulsation amplitude of the radial exciting force in

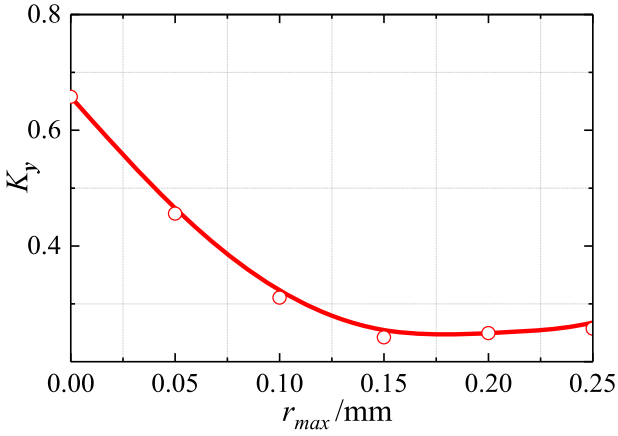


**Figure 13.** Effect of gradually varied gap on the radial force pulsation coefficient in the *y*-direction.

the *x*-direction. It can be seen that the variation of radial exciting force in the positive and negative directions of *x* is consistent. When the $r_{max} = 0$, the high-pressure side of the rotor cavity has a significant influence on the radial exciting force of the *x*-direction, with a maximum radial force of 5.4 kN. For $r_{max} = 0.1$ mm, the radial exciting force in the *x*-direction of the gradually varied gap is 4.4 kN, which is 19% lower than that of the equal gap of the rotor. With the increase of $r_{max}$ value, the pulsation amplitude of the *x*-direction radial exciting force loading on the rotor at the high-pressure end gradually decreases, and reaches $r_{max}$ minimum value of 0.15 mm, and then gradually increases. Although the force is increased, there is no obvious abrupt change and the curve transition is relatively smooth. When $r_{max} = 0.15 \sim 0.2$ mm, the effect

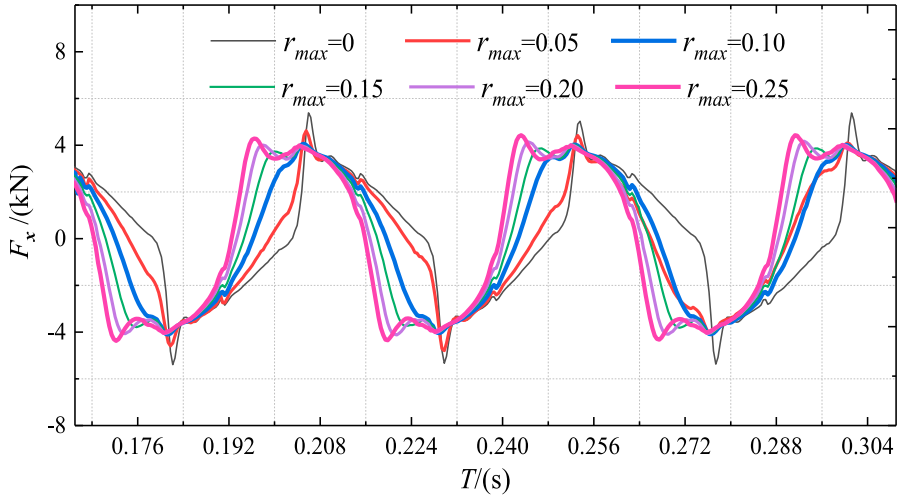


(a)

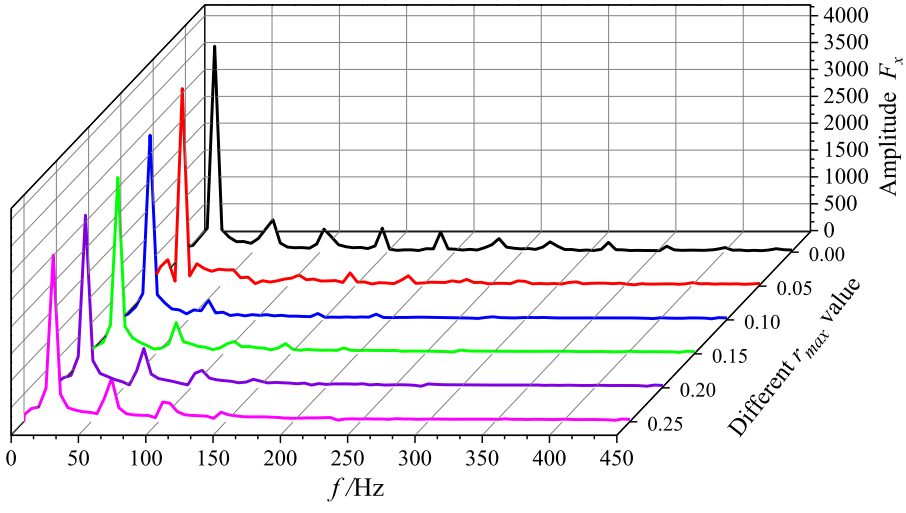


(b)

**Figure 14.** Pulsation characteristics of radial force in the *x*-direction of the rotor.

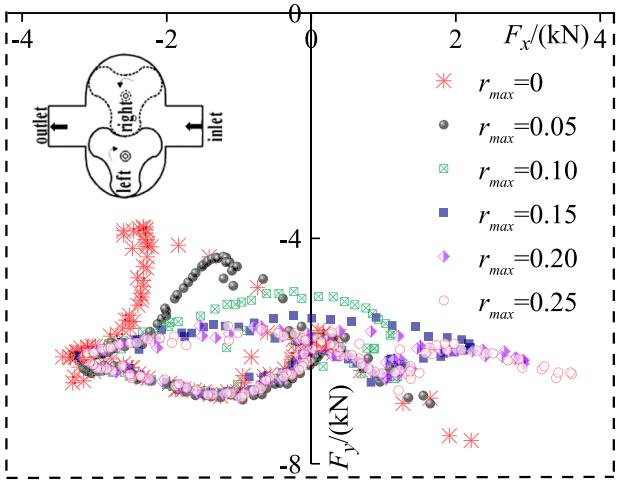


**Figure 15.** Effect of the gradually varied gap on the radial force of the left rotor in 1/6 cycle.

of $r_{max}$ value on the radial exciting force of the rotor in $x$-direction is not remarkable.

Figure 14(b) shows the frequency domain diagram of the $F_x$ pulsation of different gradually varied gap. It can be seen from the figure that the maximum amplitude of the main frequency of the monitoring point also appears at $r_{max} = 0$, and then decreases. But compared with the Figure 14(a), it can be seen that the gradually varied gap inhibition of the pulse intensity of the $F_x$ is not obvious.

Figure 15 shows the four-quadrant distribution of the radial exciting force of the left rotor of the pump (only in 1/6 cycle). It can be seen that the radial exciting force of the left rotor in the $y$-direction is twice as large as that in the $x$-direction. And the rotor is mainly affected by the radial exciting force from the negative direction of the $y$-axis. However, the radial exciting force in the $x$-direction is not limited to the change of magnitude, at the same time, the direction of the radial force is also changing, so that the $x$-direction is mainly affected by the alternating load. When the $r_{max}$ is changed in the range of $0.1 \sim 0.15$ mm, the stress distribution is more concentrated and there is no obvious pulse and the amplitude of the radial exciting force is smaller than the other values, which is consistent with the above analysis.

## 6. Conclusions

The RNG $k$–$\epsilon$ turbulence model and the dynamic mesh were used to compute the two-dimensional turbulence flow field distribution and analysis of the equal gap of the rotary lobe pump and the ones with gradually varied gap. Meanwhile, the curve of the outlet flow rate, the pressure distribution in the rotor transition chamber, and the radial exciting force on the rotor are analysed. The conclusions are as follows:

(1) There is an obvious vortex flow in the discharge process of the rotary lobe pump. The vortex flow causes a small flow disturbance at the peak of the output flow pulsation curve. The fluid at the high-pressure side of the pump with a gradually varied gap structure would begin to reflow and equalize the pressure before the closed element was opened. So that the pressure in the transition element reaches the discharge pressure in advance. Thus, the vortex disturbance, pressure and flow pulsation caused by the rapid return of high-pressure liquid can be avoided at the moment of volume opening of the transition element in the pump cavity with equal gap.

(2) When the gradually varied gap $r_{max} = 0.1$ mm, in the high-pressure side, the radial exciting force on rotor in the $y$-direction is reduced by 12% compared with that in the equal gap. And the radial exciting force pulsation coefficient is 0.31. At the same time, radial exciting force in the $x$-direction is reduced by 19% compared with that in the equal gap. Therefore, the lobe pump with gradually varied gap structure can effectively avoid the effect of the sudden change of stress on the transmission shaft system.

(3) Based on the CFD dynamic mesh technology, the influence of gradually varied gap on the radial exciting force of the rotor and its intrinsic mechanism is obtained. When the gradually varied gap $r_{max} = 0.1$ mm, the average amplitude of the flow and pressure pulsation at the outlet of the pump reaches a minimum.

Further efforts are needed to explore the transient flow inside the rotary lobe pump using photography techniques and high-speed Particle Image Velocimetry, which is considered to be more meaningful.

## Disclosure statement

No potential conflict of interest was reported by the authors.

## Funding

This work was supported by the National Natural Science Foundation of China [grant numbers 51369015 and 51866009].

## ORCID

*Dong-Sheng Guo* http://orcid.org/0000-0002-4383-6532

## References

Alemi, H., Nourbakhsh, S. A., Raisee M., & Najafi, A. F. (2015). Development of new "multivolute casing" geometries for radial force reduction in centrifugal pumps. *Engineering*

*Applications of Computational Fluid Mechanics*, *9*(1), 1–11. doi:10.1080/19942060.2015.1004787

Arjeneh, M., Kovacevic, A., Rane, S., Manolis, M. J., & Stosic, N. (2015). Numerical and experimental investigation of pressure losses at suction of a twin-screw compressor. *IOP Conference Series: Materials Science and Engineering*, *90*(1), 1–10.

Campo, D. D., Castilla, R., Raush, G. A., Montero, P. J. G., & Codina, E. (2012). Numerical analysis of external gear pumps including cavitation. *Journal of Fluids Engineering*, *134* (8): 081105. doi:10.1115/1.4007106

Costopoulos, T., Kanarachos, A., & Pantazis, E. (1988). Reduction of delivery fluctuation and optimum tooth profile of spur fear rotary pumps. *Mechanism and Machine Theory*, *23*(2), 141–146. doi:10.1016/0094-114X(88)90091-2

Dickenson, T. C. (1995). *Pumping manual* (9th ed.). New York: Elsevier Science.

FLUENT Inc. (2013). *Fluent theory guide*. New York: Ansys.Inc.

Hsieh, C. F. (2015). A new curve for application to the rotor profile of rotary lobe pumps. *Mechanism and Machine Theory*, *87*, 70–81. doi:10.1016/j.mechmachtheory.2014.12.018

Hsieh, C. F., & Hwang, Y. W. (2007). Study on the high-sealing of roots rotor with variable trochoid ratio. *Journal of Mechanical Design*, *129*(12), 1278–1284. doi:10.1115/1.2779897

Huang, Z. F., & Liu, Z. X. (2009). Numerical study of a positive displacement blower. *Proceedings of the institution of mechanical engineers, Part C: Journal of Mechanical Engineering Science*, *223*(10), 2309–2316. doi:10.1243/09544062JMES1503

Hwang, Y. W., & Hsieh, C. F. (2006). Study on high volumetric efficiency of the roots rotor profile with variable trochoid ratio. *Proceedings of the Institution of Mechanical Engineers, Part C: Journal of Mechanical Engineering Science*, *220*(9), 1375–1384. doi:10.1243/09544062JMES176

Kang, Y. H., & Vu, H. H. (2014). A newly developed rotor profile for lobe pumps: Generation and numerical performance assessment. *Journal of Mechanical Science and Technology*, *28*(3), 915–926. doi:10.1007/s12206-013-1159-7

Kethidi, M., Kovacevic, A., Stosic, N., & Smith, I. K. (2011). Evaluation of various turbulence models in predicting screw compressor flow processes by CFD. 7th International Conference on Compressors and their Systems, 347–357.

Kovacevic, A., Stosic, N., Mujic, E., & Smith, I. K. (2007). CFD integrated design of screw compressors. *Engineering Applications of Computational Fluid Mechanics*, *1*(2), 96–108. doi:10.1080/19942060.2007.11015185

Li, Y. B., Jia, K., Meng, Q. W., Shen, H., & Sang, X. H. (2013). Flow simulation of the effects of pressure angle to lobe pump rotor meshing characteristics. *IOP Conference Series: Materials Science and Engineering*, *52*(3), 1–7.

Ma, Y., Luo, H. S., Zhang, Z. H., Zhou, S. Q., & Deng, H. Y. (2017). Numerical modeling of dynamic characters for combined valves in multiphase pump. *Engineering Applications of Computational Fluid Mechanics*, *11*(1), 328–339. doi:10.1080/19942060.2017.1292409

Mimmi, G., & Pennacchi, P. (1994). Flow rate regularity in rotary trochoidal-lobe pumps. *ASME machine elements and machine dynamics, 71*, 295–302.

Mimmi, G., & Pennacchi, P. (1999). Analytical model of a particular type of positive displacement blower. *Proceedings of the Institution of Mechanical Engineers, Part C: Journal of Mechanical Engineering Science*, *213*(5), 517–526. doi:10.1243/0954406991522743

Peng, Q. L., Gui, L. J., & Fan, Z. J. (2018). Numerical and experimental investigation of splashing oil flow in a hypoid gearbox. *Engineering Applications of Computational Fluid Mechanics*, *12*(1), 324–333. doi:10.1080/19942060.2018.1432506

Sun, S. K., Jia, X. H., Xing, L. F., & Peng, X. Y. (2018). Numerical study and experimental validation of a roots blower with backflow design. *Engineering Applications of Computational Fluid Mechanics*, *12*(1), 282–292. doi:10.1080/19942060.2017.1419148

Tong, S. H., & Yang, D. C. H. (2005). Rotor profiles synthesis for lobe pumps with given flow rate functions. *Journal of Mechanical Design*, *127*(2), 287–294. doi:10.1115/1.1798271

Valdès, L. C., Barthod B., & Perron, Y.L. (1999). Accurate prediction of internal leaks in stationary dry roots vacuum pumps. *Vacuum*, *52* (4), 451–459. doi:10.1016/S0042-207X(98)00330-3

Vogelsang, H., Verhülsdonk, B., Türk, M., & Hörnig, G. (1999). Pulsation problems in rotary lobe pumps. *World Pumps*, *389*, 45–52 doi:10.1016/S0262-1762(00)87679-8

Wang, J., Jiang, X., & Cai, Y. (2015). Investigation of a novel circular arc claw rotor profile for claw vacuum pumps and its performance analysis. *Vacuum*, *111*, 102–109. doi:10.1016/j.vacuum.2014.10.003

Yakhot V., & Orszag S. A. (1986). Renormalization group analysis of turbulence. I. Basic theory. *Journal of Scientific Computing*, *1*(1), 3–51. doi:10.1007/BF01061452

Yang, D. C. H., & Tong, S. H. (2002). The specific flow rate of deviation function based lobe pumps-derivation and analysis. *Mechanism and Machine Theory*, *37*(10), 1025–1042. doi:10.1016/S0094-114X(02)00065-4

Zhang, B., Ma, J., Hong, H. C., Yang, H. Y., & Fang, Y. T. (2017). Analysis of the flow dynamics characteristics of an axial piston pump based on the computational fluid dynamics method. *Engineering Applications of Computational Fluid Mechanics*, *11*(1), 86–95. doi:10.1080/19942060.2015.1091686